

A Heteroclinic Connection between Two Saddle Slow Manifolds in the Olsen Model

Elle Musoke, Bernd Krauskopf, and Hinke M. Osinga

Department of Mathematics, University of Auckland, Private Bag 92019

Auckland, 1142, New Zealand

elle.musoke@auckland.ac.nz

Received (to be inserted by publisher)

The abstract should summarize the context, content and conclusions of the paper. It should not contain any references or displayed equations. Typeset the abstract in 10 pt Times Roman with baselineskip of 12 pt, making an indentation of 1.6 cm on the left and right margins.

Keywords: A list of 3–5 keywords are to be supplied.

1. Introduction

Slow-fast dynamical systems are characterized by certain variables that evolve on a fast time scale while other variables evolve on a slower time scale. The separation of variables into fast and slow can be found in many systems: chemical systems, neurons, electric circuits, lasers, and predator-prey dynamics, among others, have been described by slow-fast models [Brøns & Bar-Eli, 1991; De Maesschalck & Wechselberger, 2015; Van der Pol, 1927; Otto *et al.*, 2012; Piltz *et al.*, 2017]. By reason of their ubiquity, the various phenomena that arise from the multiple-time-scale nature of slow-fast systems are of significant interest. These have been described for two- and three-dimensional systems by well-established theory [Benoît *et al.*, 1981; Benoît, 1982, 1985; Guckenheimer, 1985; Brøns *et al.*, 2006; Krupa *et al.*, 2008].

In particular, we study the mechanisms responsible for the oscillatory behaviours exhibited by many slow-fast systems. In two-dimensional systems, small-amplitude limit cycles transitioning to larger-amplitude relaxation oscillations were studied, for example, in the Van der Pol oscillator and the FitzHugh–Nagumo model [Benoît *et al.*, 1981; FitzHugh, 1955]. In three-dimensional systems, periodic orbits with epochs of localized small-amplitude oscillations (SAOs) and epochs of large-amplitude oscillations (LAOs) have been observed [Hudson *et al.*, 1979]. The mechanisms that cause SAOs of these appropriately named mixed-mode oscillations (MMOs) are described in [Desroches *et al.*, 2012]. In this paper, we investigate novel phenomena that arise in four-dimensional slow-fast systems which may provide insight into undiscovered mechanisms for MMOs in higher-dimensional systems.

We consider a prototypical four-dimensional slow-fast dynamical system that exhibits MMOs, namely a so-called Olsen model for peroxidase-oxidase reaction that was first introduced by Lars F. Olsen in 1983 [Olsen, 1983]. There are many different versions of the Olsen model and we consider the one given in [Kuehn & Szmolyan, 2015]. The MMO in the Olsen model phase space is of particular interest because it does not seem to be generated by the familiar mechanisms for MMOs from three-dimensional systems.

Previous studies exploring the mechanisms for MMOs in slow fast dynamical systems investigate the role of so-called slow manifolds in MMO generation and organisation. Slow manifolds are families of tra-

jectories on which the flow evolves on the slow timescale. A slow manifold may have families of trajectories that converge toward it in forward or backward time, respectively called the stable and unstable manifolds of the slow manifold. If a slow manifolds has both a stable and an unstable manifold, it is called a saddle slow manifold. In [Hasan *et al.*, 2018], techniques were developed to compute a two-dimensional saddle slow manifolds and its two-dimensional stable and unstable manifolds in the four-dimensional Hodgkin–Huxley model. In [Harvey *et al.*, 2010] a three-dimensional slow manifold was studied to understand calcium oscillations inside cells. In [Vo *et al.*, 2013a] a four-dimensional model for a pituitary lactotrophic cell was investigated from both a two- and three-timescale viewpoints. From the two-timescale perspective, the model has a slow manifold was three dimensional. In [Mitry *et al.*, 2013] a six-dimensional model with a two-dimensional slow manifold was studied in the context of an excitable neuron. [Vo *et al.*, 2013b]

The classification of variables into those that evolve on a fast time scale and those that evolve on a slow time scale is not straightforward for the Olsen model because the variables are not consistently slow or fast over all regions of phase space. In fact, the Olsen model nominally has three different time scales. We focus specifically on a parameter regime corresponding to two different time scales with three fast and one slow variables. This parameter regime was also the focus in [Desroches *et al.*, 2009] which reports on a study of mechanisms for MMOs after a model reduction to a three-dimensional system. Two saddle slow manifolds, saddle objects on which the flow evolves on the slower time scale, were computed along with the manifolds of trajectories converging to them in forward and backward time, respectively called stable and unstable manifolds. These gave insight into the formation of MMOs, as well as the cause of their particular geometry. However, because of the assumptions used to reduce the model to a three-dimensional system, the dimensions of the stable manifold of one slow manifold and unstable manifold of the other were reduced to two in contrast to the corresponding three-dimensional manifolds in the full system.

In the full system, the three-dimensional stable manifold of one slow manifold and the unstable manifold of the other are expected to intersect generically in a two-dimensional surface of connections between the two slow manifolds. Such a surface does not generically exist in four-dimensional systems for slow manifolds of dimension larger than one. The surface of connections also does not exist generically in systems of dimension lower than three. In these cases, the stable and unstable manifolds of the saddle slow manifolds are limited to dimensions of two or lower and therefore do not typically have intersections of dimension two or higher. In this research, we develop techniques for computing the three-dimensional stable and unstable manifolds of the one-dimensional saddle slow manifolds in the Olsen model. Furthermore, we use our techniques in conjunction with Lin’s method to compute the intersection of the three-dimensional stable and unstable manifolds in the full four-dimensional model. This intersection is involved in the formation and organisation of an attracting MMO in our system and could lead to insights about the formation and organisation of MMOs in other systems.

This paper is organised as follows. In the next section we give the necessary background from geometric singular perturbation theory (GPST) for defining the three-dimensional manifolds which are the focus of this research. Section 3 gives definitions of the manifolds which are then computed in section 4. In section 5, a computation of the intersection of the manifolds computed in section 4 is described. Conclusions are given in section 6.

2. The Olsen Model

To gain a better understanding of the Olsen model’s multiple timescale structure, we consider the scaled system from [Kuehn & Szmolyan, 2015], given by the system of ordinary differential equations

$$\begin{cases} \frac{dA}{dt} = \mu - \alpha A - ABY, \\ \frac{dB}{dt} = \varepsilon(1 - BX - ABY), \\ \frac{dX}{dt} = \lambda(BX - X^2 + 3ABY - \zeta X + \delta), \\ \frac{dY}{dt} = \kappa\lambda(X^2 - Y - ABY), \end{cases} \quad (1)$$

where $(A, B, X, Y) \in \mathbb{R}^4$ are positive concentrations of chemicals. The system parameters are represented by the Greek letters appearing in (1) and these have values given in Table 1; they are chosen to be as in [Kuehn & Szmolyan, 2015] (with the minor modification, for notational convenience, of substituting ε_b with ε and ε^2 with $\frac{1}{\lambda}$).

Table 1. Parameters for system (1) as specified in [Kuehn & Szmolyan, 2015] that correspond to a system with three fast (A, X, Y) and one slow (B) variables.

α	δ	ε	λ	κ	μ	ζ
0.0912	1.2121×10^{-4}	0.0037	18.5281	3.7963	0.9697	0.9847

Throughout the parameters have the values given in Table 1, where the time-scaling parameters ε and λ are chosen so that we are dealing with a regime with three fast variables, A , X , and Y , and one slow variable, B [Kuehn & Szmolyan, 2015].

The classical analysis of slow-fast systems considers the different so-called singular limits. In the limit of $\varepsilon = 0$, system (1) reduces to

$$\begin{cases} \frac{dA}{dt} = \mu - \alpha A - ABY, \\ \frac{dX}{dt} = \frac{1}{\lambda}(BX - X^2 + 3ABY - \zeta X + \delta), \\ \frac{dY}{dt} = \frac{\kappa}{\lambda}(X^2 - Y - ABY), \end{cases} \quad (2)$$

with the condition that $\frac{dB}{dt} = 0$ so that B is a parameter. We refer to system (2) as the layer equation which is a three-dimensional system. Performing the time rescaling $\tau = \varepsilon t$ and then considering the limit of $\varepsilon = 0$ the system reduces to the differential algebraic system

$$\begin{cases} 0 = \mu - \alpha A - ABY, \\ \frac{dB}{d\tau} = (1 - BX - ABY), \\ 0 = \frac{1}{\lambda}(BX - X^2 + 3ABY - \zeta X + \delta), \\ 0 = \frac{\kappa}{\lambda}(X^2 - Y - ABY), \end{cases} \quad (3)$$

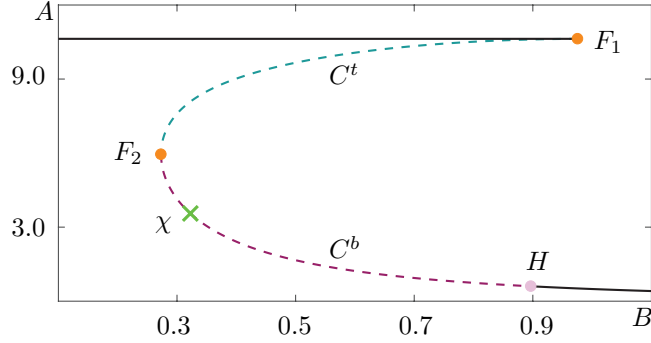


Fig. 1. Physically relevant branches of the critical manifold of system (1) shown in projection onto the (B, A) -plane. The branches labeled C^3 (teal) and C^2 (raspberry), correspond to saddle equilibria of (2), solid curves indicate stable nodes. The two saddle-node bifurcations are represented as orange dots and labeled F_1 and F_2 , respectively. The Hopf bifurcation is labeled H (pink dot). A saddle equilibrium exists on C^2 and is labeled χ (green cross).

called the reduced system. The three algebraic equations in system (3) define a one-dimensional manifold, called the critical manifold. The flow on (3) is defined by the single differential equation for B and it is confined to the critical manifold.

The critical manifold consists of equilibria of the fast subsystem (2) for different values of B . Their stability can be determined by the stable and unstable directions of the 3×3 Jacobian matrix of (2) evaluated at each point on the critical manifold. Equilibria at which the Jacobian has eigenvalues with non-zero real parts are called hyperbolic; otherwise we say that the equilibrium is non-hyperbolic. Non-hyperbolic equilibria correspond to local bifurcations of system (2).

The critical manifold is divided into branches by bifurcation points of the fast subsystem (2), the B -values for which are given to three decimal places. All points on each branch have the same number of stable and unstable directions. In our notation for branches, superscripts indicate the dimension of the space spanned by the collection of stable directions of points on the branch. Subscripts are used to distinguish the two branches on which equilibria have the same number of stable directions. Four branches of the critical manifold lie in the physically relevant region where all phase-space variables are positive. These are shown projected into the (B, A) -plane in Figure 1. The uppermost, black branch, denoted C^4_+ , consists of stable equilibria of (2). It is separated from the teal-colored branch of saddle equilibria, denoted C^3 , by a very sharp fold point F_1 , shown in orange at $B \approx 0.956$. Another fold at $B \approx 0.273$, also shown in orange and denoted F_2 , separates C^3 from a lower raspberry-colored branch of saddle equilibria. The raspberry branch of saddle equilibria is denoted C^2 . The branch C^2 ends at a Hopf bifurcation for $B \approx 0.897$, represented by the pink dot denoted H . To the right of H , in black, equilibria are stable and are collectively denoted C^4_- .

Equilibria $p \in C^3$ each have a two-dimensional stable space $E^s(p)$ and a one-dimensional linear unstable space $E^u(p)$. We denote the local stable and unstable manifolds of points p on the critical manifold by $W_{loc}^s(p)$ and $W_{loc}^u(p)$. These are the trajectories in (1) that for $\varepsilon = 0$ converge to locally p in forward and backward time, respectively. By combining these manifolds for all $p \in C^3$, we find the saddle branch C^3 has a three-dimensional local stable manifold $W_{loc}^s(C^3)$ and a two-dimensional local unstable manifold $W_{loc}^u(C^3)$ with respect to (2), which are defined as

$$W_{loc}^s(C^3) = \bigcup_{p \in C^3} W_{loc}^s(p), \quad W_{loc}^u(C^3) = \bigcup_{p \in C^3} W_{loc}^u(p).$$

Similarly C^2 has a three-dimensional local unstable manifold $W_{loc}^u(C^2)$ and a two-dimensional local stable manifold $W_{loc}^s(C^2)$ with respect to system (2).

Although the branches C^3 and C^2 of the critical manifold are no longer invariant for $\varepsilon > 0$, Fenichel Theory guarantees that both C^3 and C^2 persist as locally invariant manifolds called slow manifolds, which

are traditionally denoted by S_ε^3 and S_ε^2 [Fenichel, 1979]. For notational convenience, we drop the subscript indicating dependence on ε and use the notation S^3 and S^2 . The slow manifold S^3 has the same dimension and stability and lies at an $O(\varepsilon)$ Hausdorff distance from C^3 . For this reason, S^3 converges to C^3 as $\varepsilon \rightarrow 0$. Orbit segments that lie on a slow manifold remain slow for an $O(1)$ time with respect to the slow time scale. Due to this finite time nature, slow manifolds are not unique, however they lie exponentially close to each other. Any trajectory that remains slow for an $O(1)$ amount of slow time can be considered to be a slow manifold. We select a unique representative S^3 by considering the slow manifold that remains slow for the longest amount of time. A unique slow manifold, S^2 , associated with the critical manifold branch C^2 can be analogously defined and selected.

The stable manifold $W^s(S^3)$ of S^3 is defined as a family of orbit segments that have a fast approach to S^3 and then stay close to it for $O(1)$ time with respect to the slow time scale. According to Fenichel Theory, $W^s(S^3)$ has the same dimensions as $W_{loc}^s(C^3)$ and locally lies at an $O(\varepsilon)$ distance away from $W_{loc}^s(C^3)$. Hence, $W^s(S^3)$ is three dimensional. By reversing time and substituting C^2 for C^3 in the above definition, we can similarly define the three-dimensional unstable manifold $W^u(S^2)$ associated with S^2 . The manifolds $W^s(S^3)$ and $W^u(S^2)$ are not unique. Our selection method is described in further sections.

One equilibrium on C^2 persists for $\varepsilon > 0$ at $B \approx 0.323$ and is denoted χ . Associated with χ are two two-dimensional surfaces composed of trajectories that converge to χ in forward and backward time respectively. These are called the stable and unstable manifolds of χ and are denoted $W^s(\chi)$ and $W^u(\chi)$ respectively. The manifolds $W^s(\chi)$ and $W^u(\chi)$ can be computed through conventional methods [Krauskopf *et al.*, 2007]. To the right of $W^u(\chi)$ in the (B, A) -projection, the flow is from right to left near C^2 . To the left of $W^u(\chi)$ the flow is from left to right near C^2 . The flow of the full four-dimensional system (1) is from left to right near C^3 .

3. Saddle slow manifolds and their (Un)Stable Manifolds

Definitions of a one-dimensional saddle slow manifold and its (un)stable manifolds are given in [Farjami *et al.*, 2018] which presents algorithms for their computation in a three-dimensional system. Here we consider only the slow manifold S^3 associated with C^3 ; the slow manifold S^2 can be defined in a similar manner.

The precise definition of the slow manifold S^3 is given with respect to a closed interval $[B_{\text{in}}, B_{\text{out}}]$ for the slow variable B . The values for B_{in} and B_{out} are chosen such that the interval is contained in the interval defined by the B -coordinates of the two fold points F_1 and F_2 . Note that there is a segment in C^3 for which each point $p \in C^3$ is uniquely associated via its B -coordinate with a value $B_p \in [B_{\text{in}}, B_{\text{out}}]$. Hence, for each $B_p \in [B_{\text{in}}, B_{\text{out}}]$ there is a unique point $p = (p_A, p_B, p_X, p_Y) \in C^3$ such that $p_B = B_p$. We define a solid three-sphere $D_\delta(B_p)$ with radius δ and centre p in the three-dimensional subsection $\{(A \ B \ X \ Y) \in \mathbb{R}^4 \mid B = p_B\}$, given formally by

$$D_\delta(B_p) = \{w \in \mathbb{R}^4 \mid w_B = B_p, \|w - p\| \leq \delta\}.$$

The union $\mathcal{D} = \cup_{B_p \in [B_{\text{in}}, B_{\text{out}}]} D_\delta(B_p)$ forms a four-dimensional compact cylinder. The radius δ is small, but it needs to be at least of $O(\varepsilon)$ to ensure that S^3 lies in \mathcal{D} . The one-parameter family of orbit segments that enter \mathcal{D} via $D_\delta(B_{\text{in}})$ and exit via $D_\delta(B_{\text{out}})$ are candidates for S^3 . We impose the additional condition that S^3 must have maximal integration time in \mathcal{D} to select a unique representative.

Figure 2 shows a sketch of the unique representative, S^3 in green, in projection onto the (B, A) -plane. Sketched in purple is \mathcal{D} with the spheres $D_\delta(B_{\text{in}})$ and $D_\delta(B_{\text{out}})$ represented as disks at either end; these spheres and \mathcal{D} are for illustration.

We select and approximate a specific candidate for $W^u(S^3)$. In the lower-dimensional model considered in [Desroches *et al.*, 2009], the manifold $W^s(S^3)$ was two dimensional and computed in the region between C^3 and C^2 . We now turn to the computation of the three-dimensional manifold $W^s(S^3)$ of the full system in this same region.

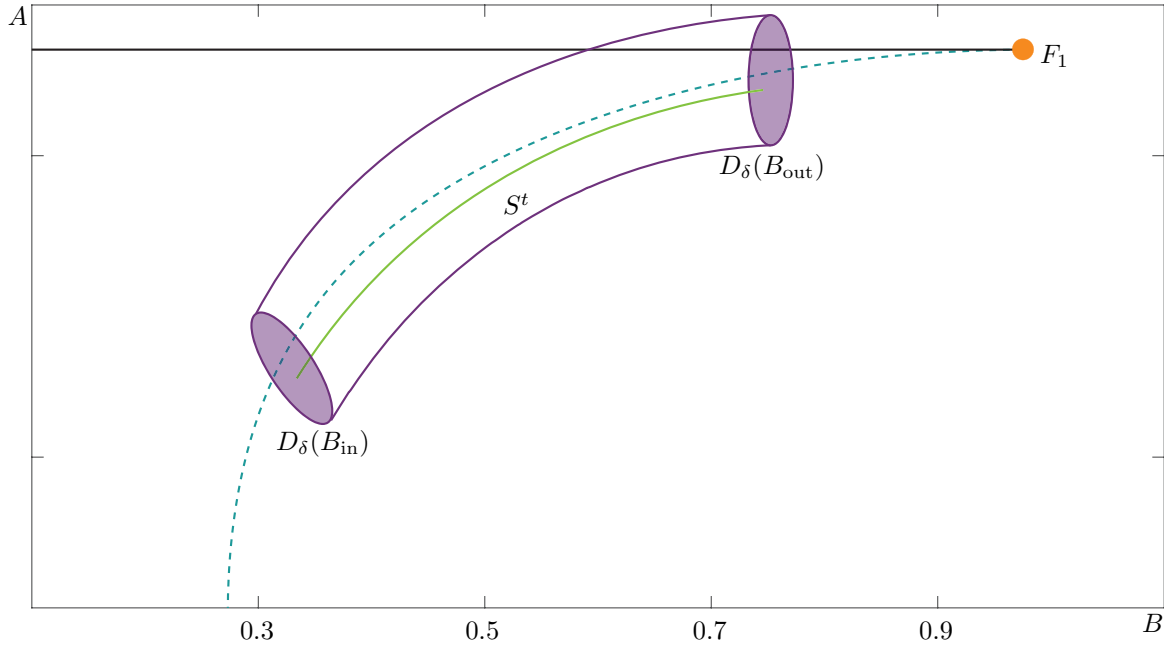


Fig. 2. The unique representative slow manifold S^3 (green curve) projected into the (B, A) -plane. The spheres $D_\delta(B_{\text{in}})$ and $D_\delta(B_{\text{out}})$ are indicated by purple disks at either end of a four-dimensional cylinder, indicated by the purple curves.

4. Computations

As $W^s(S^3)$ is three dimensional it is challenging to compute and difficult to visualise. The tools to implement the computation of three-dimensional manifolds are not widely used and, once computed, it is not possible to see the dynamics in the interior of the manifold as they are obscured by the boundary. Examples of computing and visualising three-dimensional manifolds are [Waalkens *et al.*, 2005; H\'aro & de la Liave, 2006; Jorba & Olmedo, 2009]. None of these examples are in the context of computing (un)stable manifolds of saddle slow manifolds. To our knowledge, there is no literature on the computation of three-dimensional (un)stable manifolds of saddle slow manifolds at this time. Due to the nature of the current computation tools available, computing the entire three-dimensional manifold would be computationally expensive compared to the the computation of two-dimensional manifolds. Such a three-dimensional manifold would also be difficult to visualise in any projection of the four-dimensional phase space because the interior of the manifold would be obscured by the boundary. A natural way forward is to consider a subset of $W^s(S^3)$ as a one-parameter family of two-dimensional submanifolds. These can be computed by adapting a method outlined in [Farjami *et al.*, 2018] which can then be implemented in the two-point boundary value problem (2PBVP) continuation package AUTO [Doedel, 2007]. We begin by defining a two-dimensional plane Σ that is transverse to the flow and $\bigcup_{p \in C^3} E^u(p)$ in our region of interest, given by fixed values of A and either X or Y . We approximate a submanifold with a smooth, one-parameter family of solutions to (1) with the property that they begin in Σ , enter \mathcal{D} at $D_\delta(B_p)$ for some $B_p \in [B_{\text{in}}, B_{\text{out}}]$, and remain inside \mathcal{D} for $O(1)$ slow time. We use W_Σ^s to denote the collection of those parts of the orbit segments that enter \mathcal{D} in the fast direction. The later parts that evolve mostly in the B -direction inside \mathcal{D} for $O(1)$ slow time are considered to approximate parts of S^3 . If the later part of the orbit segment includes a fast exit from \mathcal{D} , that fast part is considered as an approximation of an orbit segment lying on $W^u(S^3)$.

The computation of submanifolds of the three-dimensional unstable manifold $W^u(S^2)$ is more complex than that of $W^s(S^3)$. Two extra challenges are a saddle equilibrium, χ , of the full system lying on C^2 at $B = 0.323$ and the Hopf bifurcation of the fast subsystem at $B = 0.897$. Additional care must be taken to ensure that the computed orbits do not increase in integration time solely by approaching the saddle equilibrium's stable manifold or by following the nearby stable slow manifold backward in time. Values

for B_{in} and B_{out} are chosen such that $\chi_B < B_{\text{out}} < B_{\text{in}} < H_B$. We can then define the four-dimensional cylinder \mathcal{D} similarly to how it was defined for $W^s(S^3)$. The unstable manifold can then be defined as a two-parameter family of orbit segments composed of a collection of one-parameter families that enter \mathcal{D} at B_{in} , follow S^2 for an $O(1)$ amount of slow time and then exit at B_p for each $B_p \in [B_{\text{in}}, B_{\text{out}}]$. We modify the steps for computing two-dimensional submanifolds of $W^s(S^3)$ in order to ensure that an increase in integration time results only from a more accurate approximation of a submanifold of $W^u(S^2)$.

We now explain first how to compute a specific submanifold $W_{\Sigma^*}^s$ for the plane Σ^* , defined by the constant values $A \approx 10.6055$ and $Y \approx 0.000230006$. These values are respectively the A - and Y -coordinates of the point $p_{\text{out}} \in C^3$ that has a B -coordinate value of $B_{\text{out}} = 0.9$. We first explain the computation of $W_{\Sigma^*}^s$.

4.1. The stable manifold associated with S^3

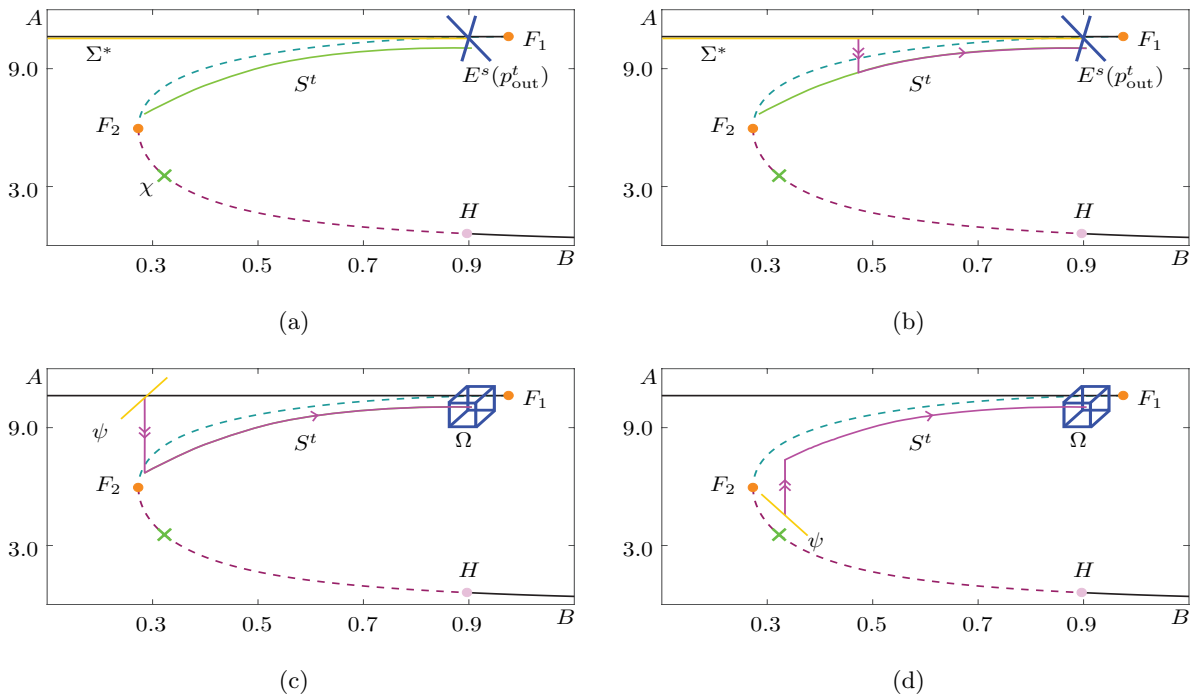


Fig. 3. Numerical set-up for the computation of submanifolds $W_{\Sigma^*}^s$ of $W^s(S^3)$. Panel (a) shows a sketch of the first homotopy step in the algorithm for computing $W_{\Sigma^*}^s$. The slow manifold S^3 is sketched in green. The plane Σ^* is given by the A - and Y -coordinates of the point p_{out} and is represented as a yellow line in the (B, A) -plane. The linear stable space $E^s(p_{\text{out}})$ is represented by a blue cross. The saddle equilibrium, χ , of the full system is represented by a green x . Panel (b) shows a representative orbit segment (purple) in the first homotopy step; fast segments are represented with double arrows while slow segments are represented with single arrows. Panel (c) shows a sketch illustrating the selection of an orbit segment (purple) with maximal integration time that ends on the blue cube Ω spanned by the two stable eigenvectors of p_{out} and the vector parallel to the B -direction; the one-dimensional subset ψ of Σ^* is given by fixing $B = B_{\text{in}}$ and represented in yellow. Panel (d) shows a sketch of the selection of a different submanifold W_{Σ}^s for Σ on the other side of the critical manifold from Σ^* with respect to the A -coordinate.

We compute the submanifold $W_{\Sigma^*}^s$ as a one-parameter family of orbit segments $\mathbf{u} = \{\mathbf{u}(s) | 0 \leq s \leq 1\}$ of the rescaled system

$$\frac{d\mathbf{u}}{ds} = TF(\mathbf{u}), \quad (4)$$

where $\mathbf{u}(s) = (A(s), B(s), X(s), Y(s)) \in \mathbb{R}^4$ is a vector of chemical concentrations, F is the right-hand side of (1) and T is the total integration time on the fast timescale, $t = Ts$.

We obtain a first solution on $W_{\Sigma^*}^s$ via a homotopy step. Following the definition for $W_{\Sigma^*}^s$, we impose the condition

$$\mathbf{u}(0) \in \Sigma^* \quad (5)$$

that is, we impose two restrictions on $\mathbf{u}(0)$ because Σ^* is two dimensional. As part of selecting an orbit segment \mathbf{u} that has a fast approach and remains close to S^3 for $O(1)$ slow time, we consider the two-dimensional eigenspace $E^s(p_{\text{out}}^t)$ that is transverse to $W^u(S^3)$. We define the boundary condition

$$\mathbf{u}(1) \in E^s(p_{\text{out}}^t) \quad (6)$$

that imposes two restrictions on $\mathbf{u}(1)$ and allows for the possibility of $\mathbf{u}(1)$ intersecting $W^u(S^3)$. The point p_{out} is a then solution to the 2PBVP defined by (4), (5) and (6) with $T = 0$. Figure 3(a) illustrates the set up for this homotopy step in projection onto the (B, A) -plane. Here, the plane Σ^* is projected to a line (yellow), $E^s(p_{\text{out}}^t)$ is represented by a blue cross, and a line representing S^3 is sketched in green. The saddle equilibrium χ is represented as a green x.

We increase the total integration time while allowing the B -coordinate value of $\mathbf{u}(0)$ to decrease towards F_2 . Note that increasing integration time in this fashion corresponds to negative T . This step is illustrated in Figure 3(b) where an intermediate orbit segment is represented as a magenta curve illustrating the presence of a fast segment (double arrows) followed by a slow segment (single arrow). The continuation is stopped just before $\mathbf{u}(0)_B$ reaches the B -coordinate value of F_2 , at $\mathbf{u}(0)_B = B_{\text{in}} = 0.275$. A sketch of the resulting orbit segment is shown in Figure 3(c).

The orbit segment illustrated in Figure 3(c) belongs to a two-parameter family of solutions \mathbf{u} of (4) that satisfy the boundary conditions (5) and (6). To select a one-parameter family of orbit segments from these, we select for each $B \in [B_{\text{in}}, B_{\text{out}}]$ the solution \mathbf{u} with maximal integration time such that $\mathbf{u}(0)_B = B$. To find an initial orbit segment satisfying this condition, we define the curve $\psi = \Sigma^* \cap \{\omega \in \mathbb{R}^4 \mid \omega_B = B_{\text{in}}\}$ and require

$$\mathbf{u}(0) \in \psi, \quad (7)$$

which imposes three conditions on $\mathbf{u}(0)$ and is more restrictive than (5). The boundary condition (7) is represented as a yellow line in Figure 3(c). We lessen the restrictions on $\mathbf{u}(1)$ and define the three-dimensional space Ω spanned by the two stable eigenvectors of p_{out} and $(0, 1, 0, 0)^{tr}$. Note that Ω is transverse to $\cup_{p \in C^3} E^u(p)$ and hence $W^u(S^3)$. Instead of (6) we require

$$\mathbf{u}(1) \in \Omega, \quad (8)$$

which imposes only one condition on $\mathbf{u}(0)$. Condition (8) is represented in Figure 3(c) as a cube with dark blue edges. We now track the solution \mathbf{u} of the 2PBVP (4), (7), (8) as T becomes more negative, forcing $\mathbf{u}(0)$ to approach $W^s(S^3) \cap \Sigma^*$ and $\mathbf{u}(1)$ to approach $W^u(S^3) \cap \Omega$. When a fold in T is reached $\mathbf{u}(0)$ and $\mathbf{u}(1)$ have intersected $W^s(S^3)$ and $W^u(S^3)$, respectively, and a (local) minimum in the total integration time T is attained.

The orbit segment that is obtained is not represented in a figure because it is almost identical to the orbit segment illustrated in Figure 3(c): it begins in Σ^* and has a fast approach to S^3 before remaining $O(\varepsilon)$ close for $O(1)$ slow time, and so it lies on $W_{\Sigma^*}^s$ by definition. In addition to finding an orbit segment that approximates a solution to (4) laying on $W_{\Sigma^*}^s$, we can approximate S^3 by restricting the orbit segment further inside $[B_{\text{in}}, B_{\text{out}}]$ to exclude fast segments. At this stage the entire solution family lying on $W_{\Sigma^*}^s$ can be computed by continuing the fold in T , while allowing $u(0)_B$ to increase.

Figure 4 shows two projections of $W_{\Sigma^*}^s$. Although the manifold is two dimensional, it is necessary to visualise it in both (B, A, X) - and (B, A, Y) -projections because it exists in four-dimensional space. Lying on $W_{\Sigma^*}^s$ is a representative orbit segment, plotted in magenta. The critical manifold is plotted and the view is rotated relative to earlier figures to help illustrate the geometry of the submanifold. Orbits lying

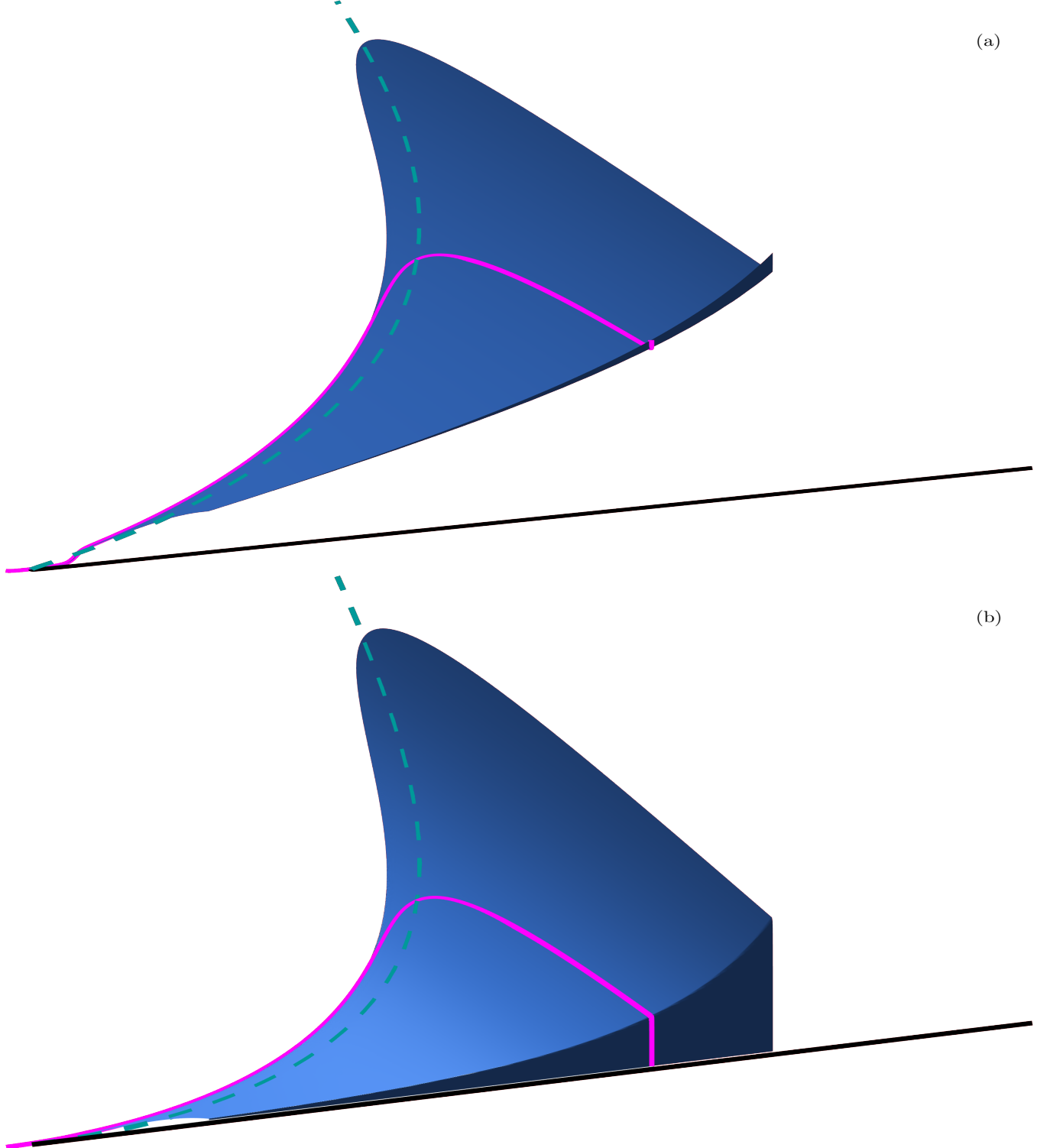


Fig. 4. The submanifold $W_{\Sigma^*}^s$ (light blue), defined as the family of orbit segments with maximal integration time that solve the 2PBVP (4), (7), (8) as B varies. Shown are projections into (B, A, X) -space (a) and (B, A, Y) -space (b) with a representative orbit segment plotted in magenta. Projections of a segment of the critical manifold are shown in turquoise and the view is rotated relative to previous figures.

on $W_{\Sigma^*}^s$ have a fast approach to S^3 in X and Y before approaching mainly in the A -direction and then finally remaining close to C^3 for $O(1)$ slow time.

In the case where we would like to compute W_{Σ}^s where Σ is defined by different constant values of

A and Y (or X), we can obtain a first orbit segment on W_Σ^s via a second homotopy step. Using an intermediate orbit segment from the first homotopy step as a starting point, we impose (6) while keeping as free parameters T , $\mathbf{u}(0)_B$, and the X -coordinate $\mathbf{u}(0)_X$ of $\mathbf{u}(0)$ (or the Y -coordinate $\mathbf{u}(0)_Y$ of $\mathbf{u}(0)$). In two runs, we continue \mathbf{u} with $\mathbf{u}(0)_A$ and $\mathbf{u}(0)_Y$ (or $\mathbf{u}(0)_X$) as main continuation parameters. In each of these runs, we increase or decrease the main continuation parameter until it attains the value necessary for $\mathbf{u}(0) \in \Sigma$. Once $\mathbf{u}(0) \in \Sigma$, we follow the rest of the procedure described above while considering Σ instead of Σ^* .

Figure 3(d) illustrates a choice of Σ on the opposite side of the critical manifold from Σ^* with respect to the A -coordinate. The orbit segment resulting from the second homotopy step is represented as a magenta curve. Conditions (7) and (8) are again illustrated with a yellow line and a cube with dark blue edges, respectively.

Figure 5 shows $W_{\Sigma^*}^s$ together with one other submanifold W_Σ^s of $W^s(S^3)$. The additional submanifold was selected with Σ given by $A = 2.0$ and $Y = 0.0$. Figure 6 shows the two submanifolds of W^s shown in Figure 5 along with three additional submanifolds. The additional submanifolds were selected with Σ given by $A = 4.0$ and $X = 0.75$, $A = 4.0$ and $Y = 0.75$, and $A = 6.0$ and $X = 0.5$. The submanifolds appear to intersect, however this is due to the variable A being slower than variables X and Y . This causes orbit segments to approach S^3 in the X - and Y -directions before approaching in the A -direction and is the reason for the portions of the submanifolds that come very near to each other.

We note that, unlike the stable manifold of S^3 computed for the reduced system in [Desroches *et al.*, 2009], each submanifold W_Σ^s in Figure 6 diverges backwards in time in the X - and Y -directions before reaching S^2 . The computations in [Desroches *et al.*, 2009] suggest that there exists a submanifold of $W^s(S^3)$ in the four-dimensional system that spirals around S^2 in backward time for an appropriate choice of Σ . Such a surface would be the intersection of the two three-dimensional manifolds $W^s(S^3)$ and $W^u(S^2)$ in the full four-dimensional system.

4.2. The unstable manifold associated with S^2

Before investigating the existence of such an intersection, we first consider the unstable manifold $W^u(S^2)$ of S^2 . The computation of submanifolds of $W^u(S^2)$ is similar to the computation of W_Σ^s , however adjustments must be made in light of the challenges described in section 4.0. Namely, we must make adjustments to boundary conditions so that orbit segments do not increase in integration time by approaching χ or by following the attracting slow manifold to the right of the Hopf bifurcation in the (B, A) -projection in backwards time. To compute a submanifold of $W^u(S^2)$, we define for each $B_p \in [B_{\text{in}}, B_{\text{out}}]$ a sphere in the subspace $\{B = B_p\}$, centered at p and with radius r ; here $p \in C^2$ is the unique point such that $p_B = B_p$. More formally,

$$\bar{D}_r(B_p) = \{w \in \mathbb{R}^4 \mid w_B = B_p, \|w - p\| = r\}.$$

We can then define the three-dimensional cylinder $\mathcal{R} = \cup_{B \in [B_{\text{in}}, B_{\text{out}}]} \bar{D}_r(B)$.

We define a submanifold W_r^u for $r > \delta$, as the one-parameter family of orbit segments that enter \mathcal{D} at B_{in} and, for each $B_p \in [B_{\text{in}}, B_{\text{out}}]$, intersect \mathcal{R} after exiting \mathcal{D} at B_p an $O(1)$ amount of slow time afterwards. The radius δ is chosen small enough so that \mathcal{R} does not contain a locus of points at which the flow is not transverse to \mathcal{R} . We use the cylinder \mathcal{R} instead of the plane Σ described in section 4.1 to keep the endpoints of orbit segments \mathbf{u} close enough to C^2 so that the \mathbf{u} cannot contain segments that approach χ . In the following steps, the computation of a submanifold $W_{r^*}^u$ is outlined for $r^* = 0.7$ before the description of the necessary modifications to obtain W_r^u for more general r .

We perform an initial homotopy step analogous to the homotopy step in section 4.1 to obtain an orbit segment that enters \mathcal{D} at B_{in} and intersects \mathcal{R} after exiting \mathcal{D} at some $B^* \in [B_{\text{in}}, B_{\text{out}}]$. We select the unique point $p^* \in C^2$ such that $p_B^* = 0.7$. The plane $\bar{\Sigma}$ is defined by fixing the A - and Y -coordinates of p^* , which are $A \approx 0.940272$ and $Y \approx 1.342954$. We impose the boundary conditions

$$\mathbf{u}(0) \in E^u(p^*), \quad (9)$$

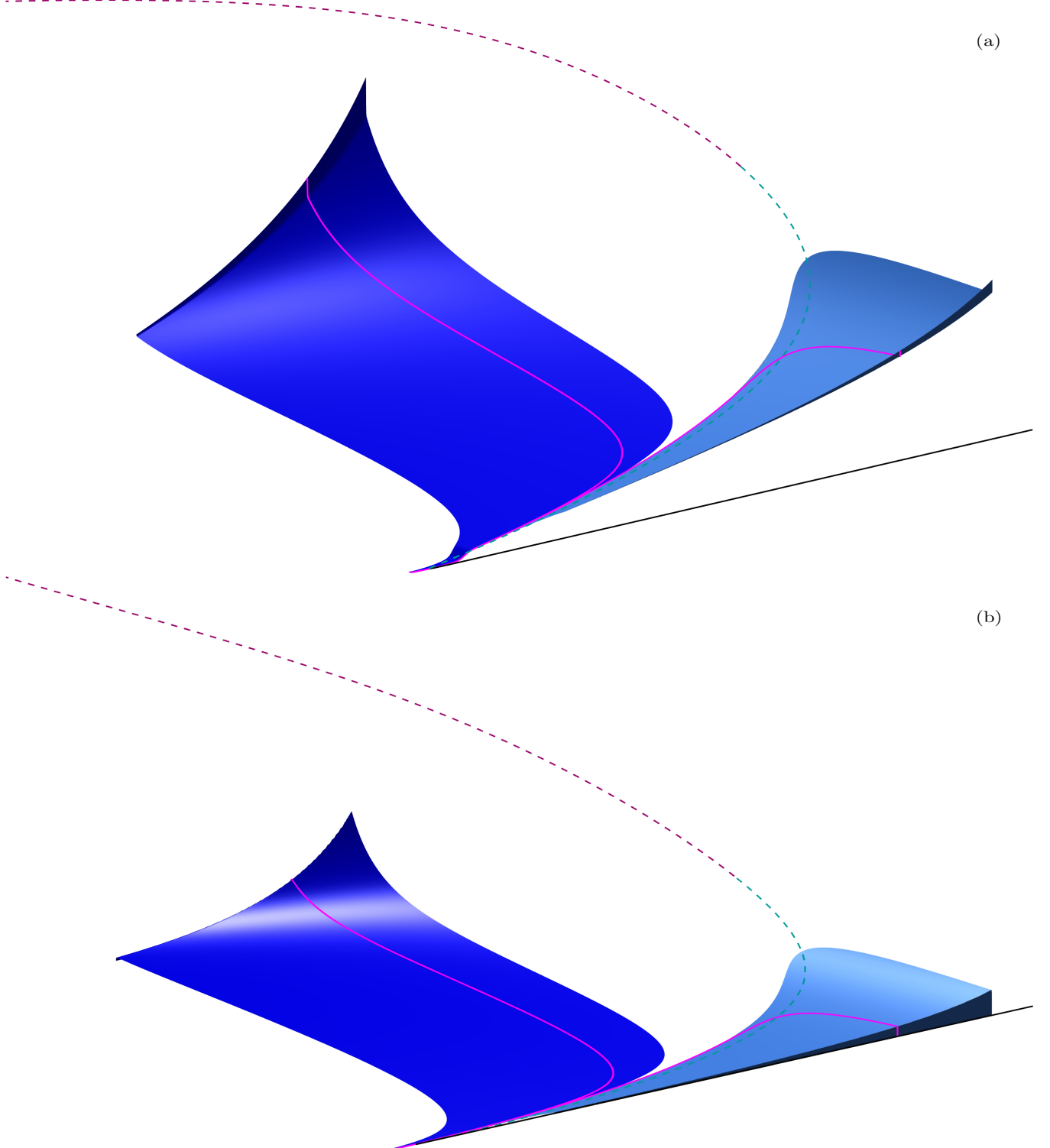


Fig. 5. The submanifolds W_Σ^s and $W_{\Sigma^*}^s$ (blue and light blue) of $W^s(S^3)$, defined as the family orbit segments with maximum integration time that solve the 2PBVP (4), (7), (8) as B varies. Here Σ is a plane defined by the constant values $A = 2.0$ and $Y = 0.0$. Shown are projections into (B, A, X) -space (a) and (B, A, Y) -space (b) with representative orbit segments plotted in magenta on each slice. Projections of the critical manifold are shown in black, turquoise, and raspberry and the view is rotated relative to previous figures.

and

$$\mathbf{u}(1) \in \bar{\Sigma} \quad (10)$$

which each impose two conditions on $\mathbf{u}(0)$ and $\mathbf{u}(1)$, respectively. The point p^* is then a solution to the 2PBVP defined by (4), (9), and (10) for $T = 0$. We increase T while $\mathbf{u}(1)_B$ decreases and stop the continuation when $\mathbf{u}(1)$ intersects \mathcal{R} . This step is almost identical to the initial homotopy step in section 4.1 except that we reverse the direction of time and instead of stopping the continuation when $\mathbf{u}(1)_B$ attains a certain value, we stop the continuation when $\mathbf{u}(1)$ intersects \mathcal{R} . We denote by B_{stop} the B -value of $\mathbf{u}(1)$ at the end of this step and p^{stop} the corresponding point in C^2 .

We perform a second homotopy step to ensure that $\mathbf{u}(0)$ is such that \mathbf{u} can approach S^2 for $O(1)$ slow time while also ensuring that \mathbf{u} doesn't increase in integration time by following the attracting slow manifold for longer backward time. In the second homotopy step we define a three-dimensional space $\Xi_{\text{HOM2}} = E^u(p^*) + \text{span}\{(0 \ B \ 0 \ 0)^{tr}\}$ and a one-dimensional circle $\Theta = \{w \in \mathbb{R}^4 \mid w_Y = p_Y^*, w_B = B_{\text{stop}}, \|w - p^{\text{stop}}\| = 0.7\}$. Then the orbit segment resulting from the first homotopy step is a solution to the 2PBVP defined by (4),

$$\mathbf{u}(0) \in \Xi_{\text{HOM2}}, \quad (11)$$

and

$$\mathbf{u}(1) \in \Theta. \quad (12)$$

Our goal is to continue the orbit segment by increasing T such that $\mathbf{u}(0)_B$ increases, that is (11) drives the continuation. Condition (12) is chosen such that integration time does not increase with decreasing $\mathbf{u}(1)_B$ and so that our 2PBVP is well defined. The continuation is stopped when $\mathbf{u}(0)_B = 1.0$. The resulting orbit segment is initially attracted to the attracting slow manifold and follows it until it passes near \mathcal{H} at which point \mathbf{u} follows S^2 . As following the attracting slow manifold for longer backwards time requires the increase of $\mathbf{u}(0)_B$, we fix $\mathbf{u}(1)_B$ from this step onwards to ensure that this does not occur. This is different from section 4.1 in which $\mathbf{u}(1)_B$ remained unfixed in the final steps of the computation.

To fix $\mathbf{u}(0)_B$, we define the plane $\Phi = \{w \in \Xi_{\text{HOM2}} \mid w_B = 1.0\}$ and impose the boundary conditions

$$\mathbf{u}(0) \in \Phi, \quad (13)$$

and

$$\mathbf{u}(1) \in \{w \in \mathcal{R} \mid w_B = B_{\text{stop}}\}. \quad (14)$$

Condition (14) requires that $\mathbf{u}(1)$ remain on a two-dimensional sphere as opposed to the one-dimensional curve ψ described for condition (7) in section 4.1. We must allow this extra degree of freedom for $\mathbf{u}(1)$ as keeping $\mathbf{u}(0)_B$ fixed in condition (13) imposes an extra constraint compared to condition (8) in section 4.1. Our aim is to select a smooth one-parameter family of orbit segments from the two-parameter family of orbit segments satisfying the 2PBVP defined by (4), (13), and (14) to which the orbit segment resulting from the second homotopy step is a solution. To this end, for each $B_p \in [B_{\text{in}}, B_{\text{out}}]$, we select from the one-parameter family of orbit segments exiting \mathcal{D} at B_p the orbit segment with maximal integration time. To find an initial orbit of this description we increase T again until maximal integration time is reached. This is detected as a fold in T . Finally to obtain the rest of the submanifold $W_{r^*}^u$ we switch the endpoint boundary condition to

$$\mathbf{u}(1) \in \mathcal{R} \quad (15)$$

which imposes one condition on $\mathbf{u}(1)$. In two runs, the fold in T is continued until $\mathbf{u}(0)_B = B_{\text{out}} = 0.35$ and then again until $\mathbf{u}(0)_B = B_{\text{in}} = H_B$ to sweep out $W_{r^*}^u$.

Figure 7 shows two projections of the submanifold $W_{r^*}^u$. Example orbit segments lying on $W_{r^*}^u$ are plotted in forest green and a subset of C^2 is plotted in raspberry. The view is rotated relative to previous figures.

We can compute a different submanifold W_r^u by returning to the second homotopy step in our computation. Depending on the magnitude of r , we may need to perform one or two additional homotopy steps. In the case where r is large enough that $\bar{D}_r(\mathbf{u}(1)_B)$ contains a locus of points at which the flow is not transverse to it, an extra homotopy step is needed. We define a plane Ξ_{hom3} by fixing the A - and X -coordinates of $\mathbf{u}(1)$ after the second homotopy step. To ensure that our 2PBVP is well defined, the orbit segment is continued with the boundary conditions (13) and

$$\mathbf{u}(1) \in \Xi_{\text{hom3}}, \quad (16)$$

which imposes two conditions on $\mathbf{u}(1)$. The endpoint B -coordinate $\mathbf{u}(1)_B$ is increased until $\bar{D}_r(\mathbf{u}(1)_B)$ no longer contains a locus of tangent points.

The final homotopy step involves defining another plane Ξ_{homfinal} by fixing the B - and X -values of $\mathbf{u}(1)$. Condition (13) is imposed while a new restriction

$$\mathbf{u}(1) \in \Xi_{\text{homfinal}}, \quad (17)$$

imposes two conditions on $\mathbf{u}(1)$. The radius r is then increased or decreased until the desired magnitude is attained. All that remains is to follow through with the rest of the steps to compute W_r^u . In the last step, B_{out} is chosen such that the flow is transverse to $\bar{D}(B_{\text{out}})$. We do not show several submanifolds of $W^u(S^2)$ in the same figure, because the spiralling dynamics near C^2 make visualisation difficult in the (B, A, X) - and (B, A, Y) -projections due to (self)-intersections of the submanifolds in these projections.

5. A heteroclinic connection between two saddle slow manifolds

The intersection of $W^s(S^3)$ and $W^u(S^2)$ is a two-dimensional manifold of heteroclinic connections which we denote \mathcal{H} . We can compute such a surface of connections with an approach known as Lin's method [Lin, 1989; Krauskopf & Rieß, 2008; Zhang *et al.*, 2012]. Since Lin's method is typically used in parameter continuation of heteroclinic connections that are not structurally stable, we explain the set-up here for our context. We first choose a three-dimensional so-called Lin section \mathcal{L} that divides the four-dimensional phase space into two regions such that S^3 lies in one region and S^2 is in the other. We then compute an orbit segment \mathbf{u} lying on $W^s(S^3)$ and continue it in several homotopy steps until $\mathbf{u}(0) \in \mathcal{L}$. We also compute an orbit segment \mathbf{w} on $W^u(S^2)$ and continue it until $\mathbf{w}(1) \in \mathcal{L}$ as well.

In our computations of \mathbf{u} and \mathbf{w} we do not find the orbit segments with maximal integration time as it is not straightforward to track two folds simultaneously with the automatic fold continuation in the package AUTO [Doedel, 2007]. A discussion of the numerical accuracy of our results follows in the next section. Since we are not requiring that \mathbf{w} satisfy the condition of maximal integration time, we do not run into the same issues encountered in section 4.2 for the computation of a submanifold of $W^u(S^2)$. For this reason we may compute \mathbf{w} without considering the distance of $\mathbf{w}(1)$ from C^2 .

We define a vector $\mathbf{v}_Z \in \mathbb{R}^4$ called a Lin vector and given by

$$\mathbf{v}_Z = \frac{\mathbf{u}(0) - \mathbf{w}(1)}{\|\mathbf{u}(0) - \mathbf{w}(1)\|} \quad (18)$$

as well as two unit normal vectors $\mathbf{n}_1, \mathbf{n}_2 \in \mathcal{L}$ such that $\mathbf{n}_i \perp \mathbf{v}_Z$ for $i = 1, 2$ and $\mathbf{n}_1 \perp \mathbf{n}_2$. While our choice for the vector \mathbf{v}_Z , and normal vectors \mathbf{n}_1 and \mathbf{n}_2 is arbitrary, their selection remains fixed for the remainder of the computation. The span of \mathbf{v}_Z defines a one-dimensional $z \subseteq \mathcal{L}$ called a Lin space. The distance between $\mathbf{u}(0)$ and $\mathbf{w}(1)$ in Z defines a function η called a Lin gap. We approximate an orbit segment on \mathcal{H} by continuation in the direction of decreasing η while requiring $\mathbf{u}(0), \mathbf{w}(1) \in Z$. Each time when $\eta = 0$, an orbit segment on \mathcal{H} is detected as the solution \mathbf{w} followed by \mathbf{u} at this continuation step.

5.1. Computing an initial orbit segment on $W^s(S^3)$

We choose $\mathcal{L} = \{\omega \in \mathbb{R}^4 \mid \omega_A = 6.0\}$, which is an A -coordinate in between the A -coordinates of χ and of the point on C^3 with the same B -coordinate as χ . Taking \mathcal{L} to be the section given by an A -coordinate value between these two allows us to compute the largest possible portion of \mathcal{H} without being limited by the intersection of \mathcal{L} with C^3 or C^2 .

We compute the orbit segment \mathbf{u} as in the computation of an initial orbit segment on a submanifold W_Σ^s in section 4.1 with the exception that we omit last the step to find the orbit segment with maximal integration time. Here, Σ is the plane given by $A = 6.0$ and $Y \approx 1.342954$.

5.2. Computing an initial orbit segment on $W^u(S^2)$

We perform three homotopy steps to obtain an initial orbit segment on $W^u(S^2)$. We begin with the point p^* that is a solution to the 2PBVP defined by (4), (9), and (10). We obtain an orbit segment \mathbf{w} by imposing conditions (9) and (10) while increasing integration time. The continuation is stopped when $\mathbf{w}(1)_B = 0.6$.

We then impose (11) and (10) while additionally requiring $\mathbf{w}(1)_B = 0.6$. We continue \mathbf{w} while increasing integration time once more while $\mathbf{w}(0)_B$ increases, and stop the continuation when $\mathbf{w}(0)_B = 1.0$.

In the third homotopy step, we impose (13) while keeping $\mathbf{w}(0)_B$, $\mathbf{w}(1)_B$ and $\mathbf{w}(1)_Y$ fixed. The A -coordinate of $\mathbf{w}(1)$ increases as T is increased. The continuation is stopped when $\mathbf{w}(1)_A = 6.0$. In other words, we stop the continuation when $\mathbf{w}(1) \in \mathcal{L}$.

5.3. Finding a initial orbit segment on \mathcal{H}

We are now in a position to define vectors \mathbf{v}_Z , \mathbf{n}_1 , and \mathbf{n}_2 . We define \mathbf{v}_Z using the orbit segments \mathbf{u} and \mathbf{w} obtained in sections 5.1 and 5.2 and take $\mathbf{n}_1 = (0, 0, \mathbf{v}_{Z_Y}, -\mathbf{v}_{Z_X})^{tr}$, and $\mathbf{n}_2 = (0, \mathbf{v}_{Z_Y}, 0, -\mathbf{v}_{Z_B})^{tr}$. We impose conditions

$$\begin{aligned} \mathbf{u}(0), \mathbf{w}(1) &\in \mathcal{L}, \\ [\mathbf{u}(0) - \mathbf{w}(1)] \cdot \mathbf{n}_1 &= 0, \\ [\mathbf{u}(0) - \mathbf{w}(1)] \cdot \mathbf{n}_2 &= 0 \end{aligned} \tag{19}$$

to restrict $[\mathbf{u}(0) - \mathbf{w}(1)] \in Z$. Additionally, we impose conditions (6) and (13) while allowing the integration times of \mathbf{u} and \mathbf{w} to move freely. The pair of orbit segments \mathbf{u} and \mathbf{w} obtained at the end of section 5.2 are one of a two-parameter family of orbit-segment pairs satisfying (6), (13), and (19). To formulate a well-defined 2PBVP, we impose the restriction

$$\mathbf{w}(1)_B \in \{\omega \in \mathbb{R}^4 \mid \omega_B = 0.6\}, \tag{20}$$

and continue \mathbf{u} and \mathbf{w} while η is decreased. We stop the continuation as soon as $\eta = 0$, at which point the concatenation of \mathbf{w} with \mathbf{u} forms an approximation of a heteroclinic connection in \mathcal{H} .

To obtain a one-parameter family of concatenations approximating \mathcal{H} , we require $\eta = 0$ while relaxing condition (20). We then decrease $\mathbf{w}(1)_B$ and stop the continuation before \mathbf{u} and \mathbf{w} reach the intersection of \mathcal{H} with $W^u(\chi)$. We sweep out the other side of the manifold by continuation in the opposite direction (of increasing $\mathbf{w}(1)_B$) and stop just before $\mathbf{w}(1)_B$ reaches the B -coordinate of the Hopf bifurcation point H on C^2 .

Figure 9 shows \mathcal{H} projected into (B, A, X) - and (B, A, Y) -space. The portion of \mathcal{H} composed of the collection of orbit segments \mathbf{w} is colored in red and the portion composed of orbit segments \mathbf{u} is blue. Orbit segments on \mathcal{H} spiral around S^2 for an $O(1)$ amount of slow time before exiting via $W^u(S^2)$ and following S^3 for an $O(1)$ amount of slow time via $W^s(S^3)$. Three representative orbit segments are shown, their \mathbf{w} segments in magenta and their \mathbf{u} segments in forest green.

5.4. stuff left to talk about later on

- A heteroclinic connection between two saddle slow manifolds is not a phenomenon that can occur in structurally stable three-dimensional systems. [?]
- accuracy of methods

References

- Benoît, E. [1982] “Systèmes lents-rapides dans \mathbb{R}^3 et leurs canards,” *Proceedings of the Third Schnepfenried Geometry Conference* **2**, 159–191.
- Benoît, E. [1985] “Enlacements de canards,” *Comptes Rendus Mathematique Academie des Sciences* **300**, 225–230.
- Benoît, E., Callot, J. F., Diener, F. & Diener, M. [1981] “Chasse au canard,” *Collectanea Mathematica* **31**, 37–119.
- Brøns, M. & Bar-Eli, K. [1991] “Canard explosion and excitation in a model of the Belousov-Zhabotinskii reaction,” *Journal of Physical Chemistry A* **95**, 8706–8713.
- Brøns, M., Krupa, M. & Wechselberger, M. [2006] “Mixed mode oscillations due to the generalized canard phenomenon,” *Fields Institute Communications* , 39–63.
- De Maesschalck, P. & Wechselberger, M. [2015] “Neural Excitability and Singular Bifurcations.” *The Journal of Mathematical Neuroscience* **5**.
- Desroches, M., Guckenheimer, J., Krauskopf, B., Kuehn, C., Osinga, H. & Wechselberger, M. [2012] “Mixed-Mode Oscillations with Multiple Time Scales.” *SIAM Review* **54**, 211–288.
- Desroches, M., Krauskopf, B. & Osinga, H. [2009] “The geometry of mixed-mode oscillations in the Olsen model for peroxidase-oxidase reaction.” *Discrete & Continuous Dynamical Systems* **2**, 807–827.
- Doedel, E. [2007] *AUTO-07p: Continuation and Bifurcation Software for Ordinary Differential Equations*, URL <http://indy.cs.concordia.ca/auto/>, with major contributions from A.R. Champneys, F. Dercole, T.F. Fairgrieve, Y.A. Kuznetsov, R.C. Paffenroth, B. Sandstede, X. Wang and C. Zhang.
- Farjami, S., Kirk, V. & Osinga, H. [2018] “Computing the Stable Manifold of a Saddle Slow Manifold.” *SIAM Journal on Applied Dynamical Systems* **17**, 350–379.
- Fenichel, N. [1979] “Geometric singular perturbation theory for ordinary differential equations,” *Journal of Differential Equations* **31**, 53–98.
- FitzHugh, R. [1955] “Mathematical models of threshold phenomena in the nerve membrane,” *The bulletin of mathematical biophysics* **17**, 257–278.
- Guckenheimer, J. [1985] “Singular hopf bifurcation in systems with two slow variables,” *SIAM Journal on Applied Dynamical Systems* **7**, 1355–1377.
- Háro, A. & de la Liave, R. [2006] “A parameterization method for the computation of invariant tori and their whiskers in quasi-periodic maps: Rigorous results,” *Journal of Differential Equations* **228**, 530–579.
- Harvey, E., Kirk, V., Osinga, H., Sneyd, J. & Wechselberger, M. [2010] “Understanding anomalous delays in a model of intracellular calcium dynamics,” *Chaos: An Interdisciplinary Journal of Nonlinear Science* **20**.
- Hasan, C., Krauskopf, B. & Osinga, H. [2018] “Saddle slow manifolds and canard orbits in \mathbb{R}^4 and application to the full Hodgkin-Huxley model,” *Journal of Mathematical Neuroscience* **8**.
- Hudson, J. L., Hart, M. & Marinko, D. [1979] “An experimental study of multiple peak periodic and nonperiodic oscillations in the Belousov-Zhabotinskii reaction,” *The Journal of Chemical Physics* **71**, 1601–1606.
- Jorba, A. & Olmedo, E. [2009] “On the computation of reducible invariant tori on a parallel computer,” *SIAM Journal on Applied Mathematics* **8**, 1382–1404.
- Krauskopf, B., Osinga, H. & Galán-Vioque [2007] *Numerical continuation methods for dynamical systems* (Springer International Publishing).
- Krauskopf, B. & Rieß, T. [2008] “A lin’s method approach to finding and continuing heteroclinic connections involving periodic orbits,” *Nonlinearity* **21**, 1655–1690.
- Krupa, M., Popović, N. & Kopell, N. [2008] “Mixed-mode oscillations in three time-scale systems: A

- prototypical example,” *SIAM Journal on Applied Dynamical Systems* , 361–420.
- Kuehn, C. & Szmolyan, P. [2015] “Multiscale Geometry of the Olsen Model and Non-classical Relaxation Oscillations.” *Journal of Nonlinear Science* **25**, 583–629.
- Lin, X. [1989] “Shadowing lemma and singularly perturbed boundary value problems,” *SIAM Journal of Applied Mathematics* **49**, 26–54.
- Mitry, J., McCarthy, M., Kopell, N. & Wechselberger, M. [2013] “Excitable neurons, firing threshold manifolds and canards,” *The journal of mathematical neuroscience* **3**.
- Olsen, L. [1983] “An enzyme reaction with a strange attractor.” *Physics Letters A* **94**, 454–457.
- Otto, C., Ludge, K., Vladimirov, A. G., Wolfrum, M. & Scholl, E. [2012] “Delay-induced dynamics and jitter reduction of passively mode-locked semiconductor lasers subject to optical feedback,” *New Journal of Physics* **14**.
- Piltz, S. H., Veerman, F., Maini, P. K. & Porter, M. A. [2017] “A predator–2 prey fast–slow dynamical system for rapid predator evolution,” *SIAM Journal on Applied Dynamical Systems* **16**, 54–90.
- Van der Pol, B. [1927] “Forced oscillations in a circuit with non-linear resistance. (Reception with reactive triode).” *The London, Edinburgh, and Dublin Philosophical Magazine and Journal of Science* **3**, 65–80.
- Vo, T., Bertram, R. & Wechselberger, M. [2013a] “Multiple geometric viewpoints of mixed mode dynamics associated with pseudo-plateau bursting,” *SIAM Journal on Applied Dynamical Systems* **12**.
- Vo, T., Tabak, J., Bertram, R. & Wechselberger, M. [2013b] “A geometric understanding of how fast activating potassium channels promote bursting in pituitary cells,” *Journal of Computational Neuroscience* **36**.
- Waalkens, H., Burbanks, A. & Wiggins, S. [2005] “A formula to compute the microcanonical volume of reactive initial conditions in transition state theory,” *Journal of Physics A: Mathematical and General* **38**, L759–L768, URL <http://stacks.iop.org/0305-4470/38/i=45/a=L03>.
- Zhang, W., Krauskopf, B. & Kirk, V. [2012] “How to find a codimension-one heteroclinic cycle between two periodic orbits,” *Discrete and Continuous Dynamical Systems* **32**, 2825–2851.

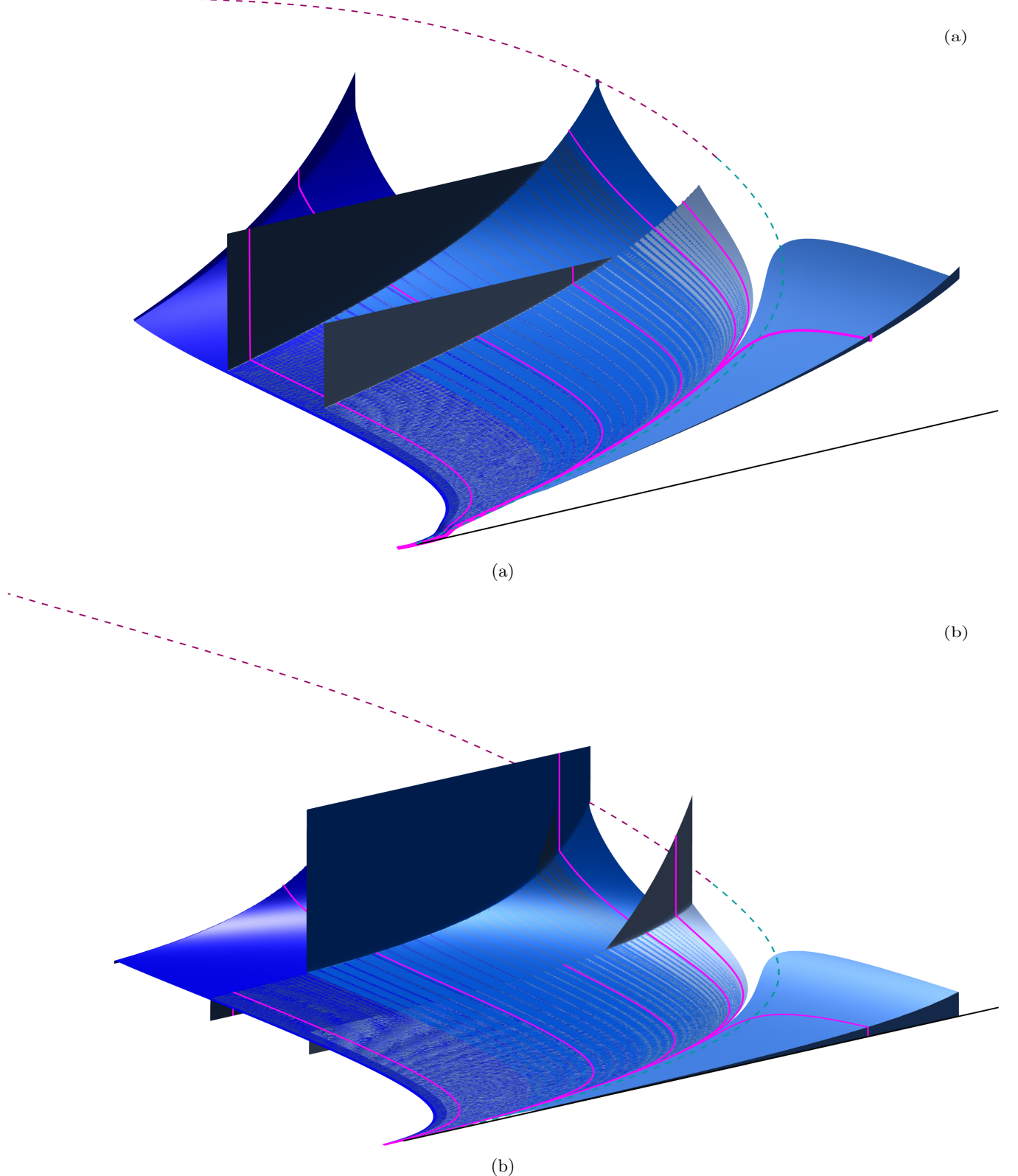


Fig. 6. The submanifold $W_{\Sigma^*}^s$ and a selection of four additional W_{Σ}^s (blues), defined as the family orbit segments with maximum integration time that solve the 2PBVP (4), (7), (8) as B varies. Here, the Σ are the planes defined by the constant values $A = 2.0$ and $Y = 0.0$, $A = 4.0$ and $Y = 0.75$, $A = 4.0$ and $X = 0.75$, and $A = 6.0$ and $X = 0.5$. Shown are projections into (B, A, X) -space (a) and (B, A, Y) -space (b) with example orbit segments plotted in magenta. Projections of the critical manifold are shown in black, turquoise, and raspberry and the view is rotated relative to previous figures.

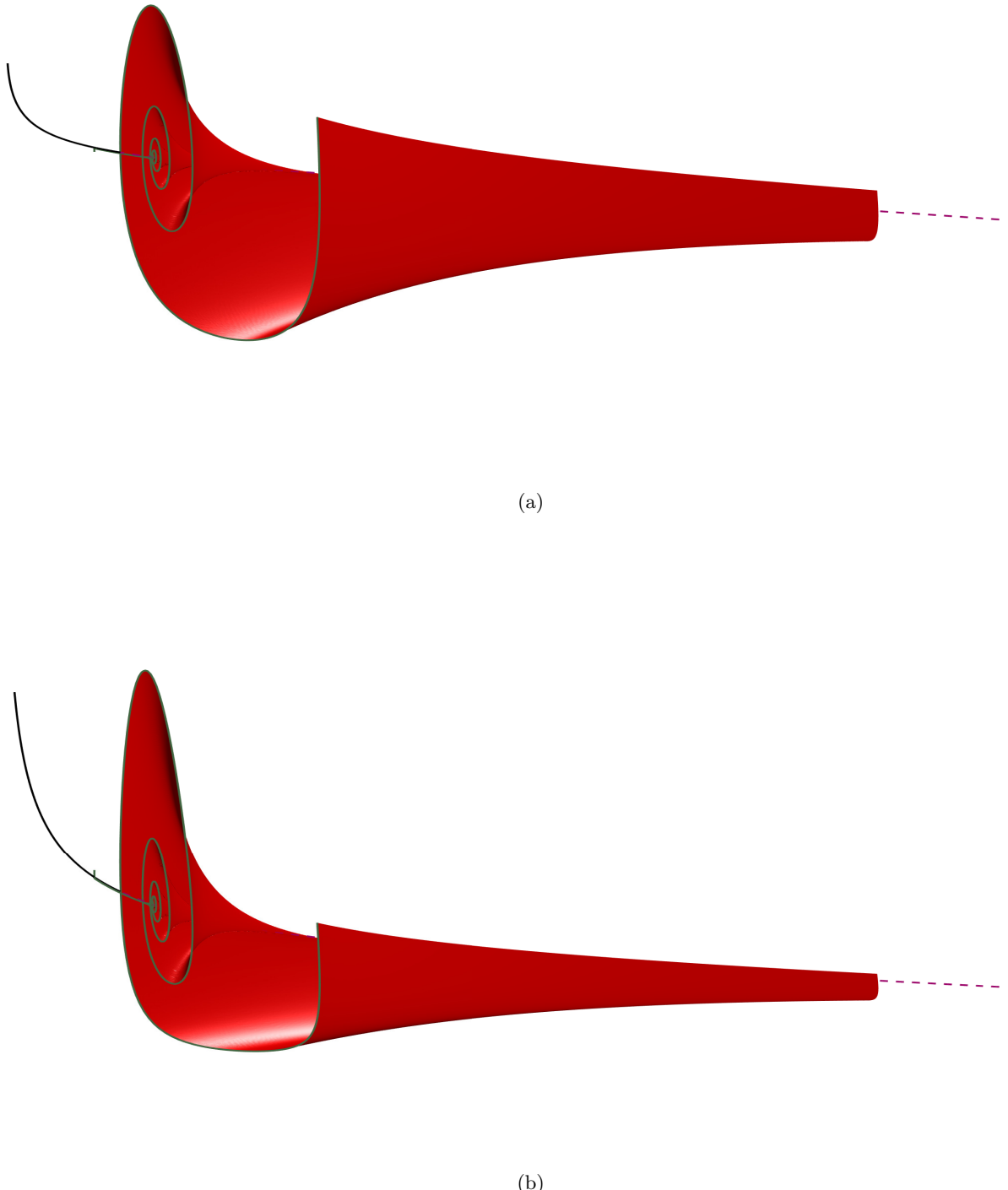


Fig. 7. The submanifold $W_{r^*}^u$ (red) of $W^u(S^2)$ computed as the family of orbit segments with maximal integration time that are solutions to the 2PBVP (4), (13), and (15) projected into (B, A, X) -space (a) and (B, A, Y) -space (b) with example orbit segments plotted in forest green. Projections of a segments of the critical manifold are shown in black and raspberry and the view is rotated relative to previous figures.

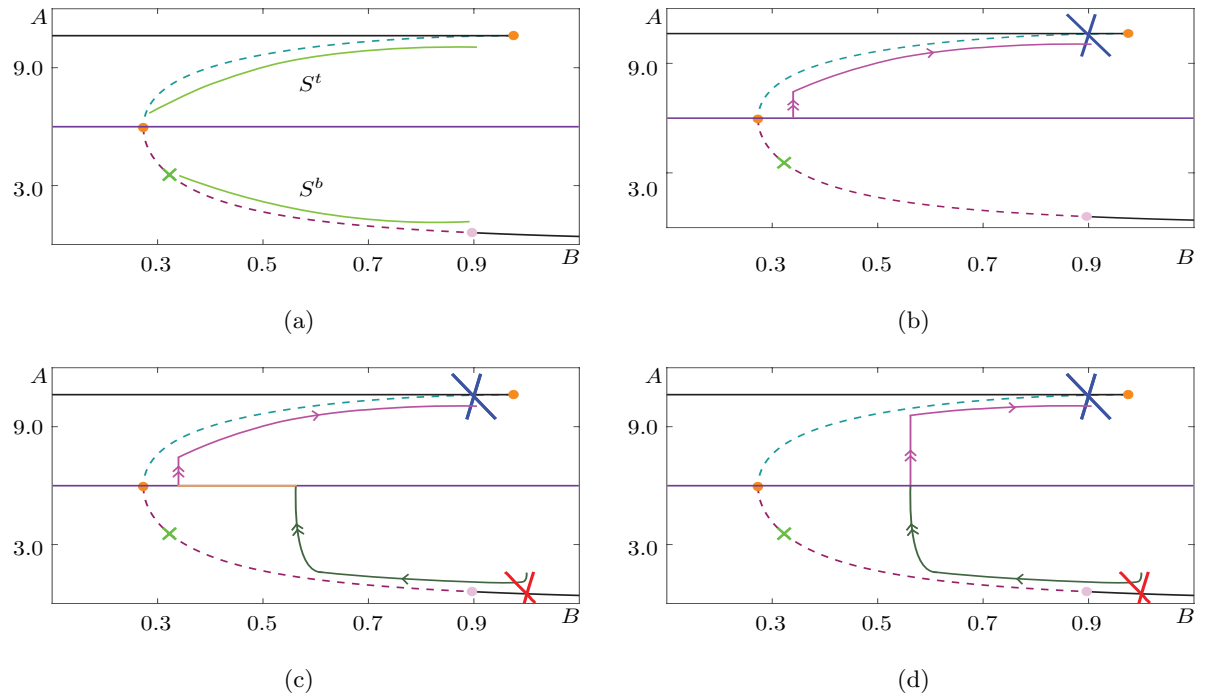


Fig. 8.

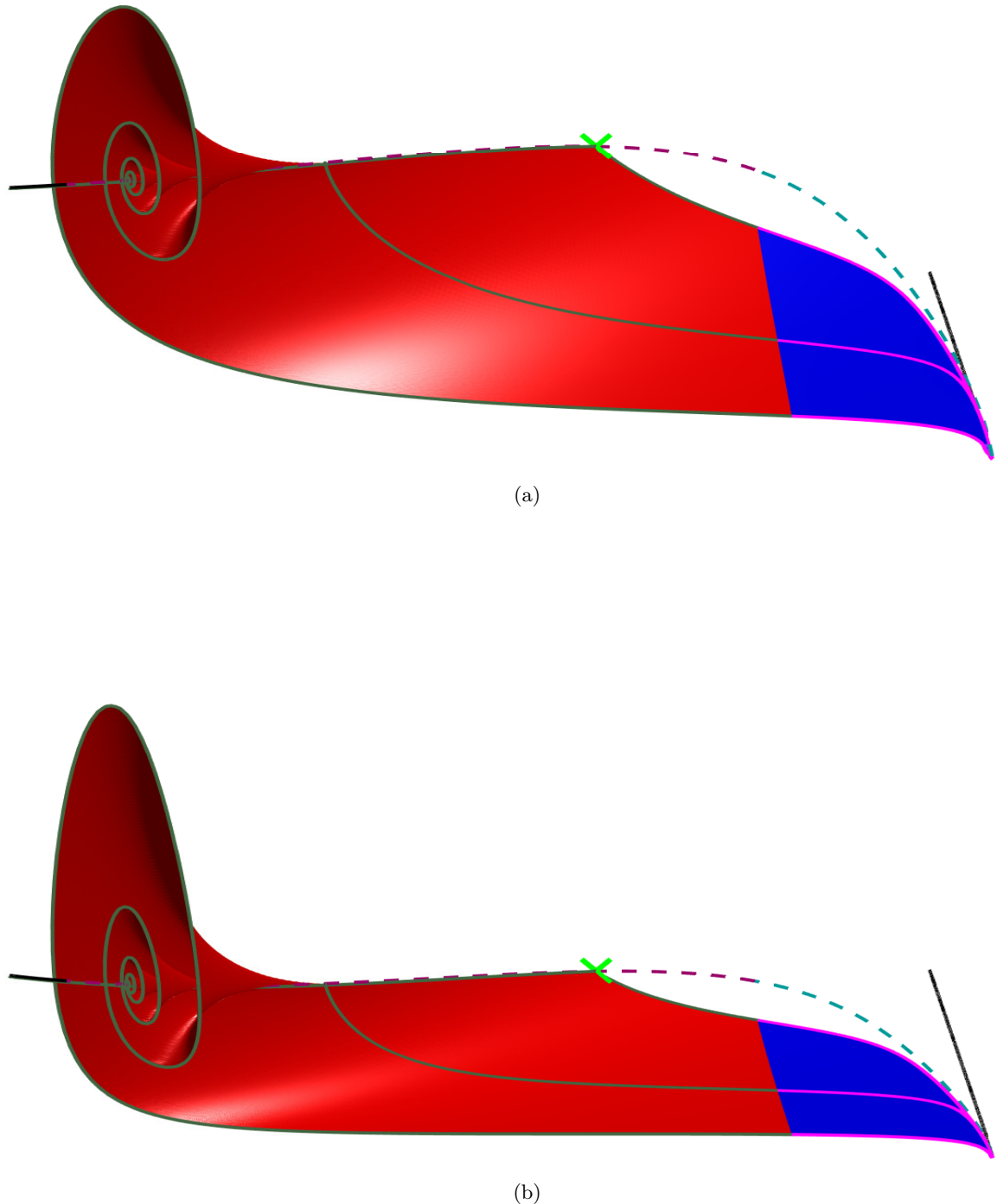


Fig. 9. The heteroclinic connection \mathcal{H} projected into (a) (B, A, X) - and (b) (B, A, Y) -space. The portion of \mathcal{H} that was computed as orbit segments in $W^s(S^3)$ is plotted in blue while the portion that was computed as orbit segments laying on W^u associated with S^2 is plotted in red. Three representative orbit segments laying on \mathcal{H} are plotted. The portions of the orbit segments computed as \mathbf{u} are plotted in magenta while the segments that were computed as \mathbf{w} are plotted in forest green. The saddle equilibrium is plotted as a green cross, partially obstructed by \mathcal{H} . The critical manifold is plotted and the view is rotated relative to previous figures to facilitate viewing.